Auxiliary material for

Earthquake clusters in southern California II: Classification and relation to physical properties of the crust

Ilya Zaliapin[1] and Yehuda Ben-Zion[2]

[1]Department of Mathematics and Statistics, University of Nevada, Reno, 89557 (zal@unr.edu)

[2] Department of Earth Sciences, University of Southern California, Los Angeles, 90089-0740 (benzion@usc.edu)

J. Geophys. Res.

Section A. *Stability of family structure with respect to the magnitude cutoff*

The goal of this section is to (i) further illustrate the dominant family types and (ii) explore stability of the family type with respect to the magnitude threshold of the analysis. We consider here two families and study how they transform depending on the minimal magnitude of the analysis. The first family is located in the Salton trough area (Fig. A1). The largest event in this family has mainshock magnitude 5.75 and coordinates (33.0875N, 115.6195W). The second family spans the San Gabriel valley and mountains (Fig. A2). The mainshock of this family has magnitude 5.51 and coordinates (34.1380N, 117.7082W); it occurred right off the San Gabriel mountains near Claremont, CA.

When the nearest-neighbor analysis is done for earthquakes with $m \geq 4.0$, the Salton trough sequence consists of a single event (Fig. A1a,b,c), while the San Gabriel family (Fig. A2a,b,c) combines 6 events in a spray-like configuration with a single foreshock.

When the magnitude cutoff in the nearest-neighbor analysis is lowered to 3.0, the number of events in both the families increases. The Salton trough family (Fig. A1d,e,f) now has 31 events, including 12 foreshocks and 18 aftershocks. The topology of the family (Fig. A1f) combines a chain of 10 events and a burst of 15 events. The San Gabriel family (Fig. A2d,e,f) now contains 34 events; and still has a single foreshock. It must be noted that the foreshock that was present in the $m \geq 4.0$ analysis no longer belongs to the cluster; such reshuffling of the nearest-neighbor cluster structure may occur even in conventional Euclidean spaces. The number of events that change their clusters under changing the magnitude cutoff of the analysis is however very small. The events in the Salton trough family are organized in a prominently spray-like shape (Fig. A2e,f), with 26 out of 34 earthquakes being direct aftershocks of the largest event. The spatial extent of the San Gabriel family (Fig. A2e) is smaller than that of the Salton trough family (Fig. A1e).

Finally, we decrease the magnitude cutoff to 2.0. The Salton trough family (Fig. A1g,h,i) now has 315 events, with 81 foreshocks and 233 aftershocks. Topologically (Fig. A1i), the family consists of multiple chains and a dominant burst that includes 136 events (43%). The San Gabriel family (Fig. A2g,h,i) has 400 events, with 3 foreshocks and 396 aftershocks. Topologically (Fig. A2i), the family is mainly comprised of a burst that includes 261 events (65%). It is now clearly seen that the spatial extend of the San Gabriel family (Fig. A2h) is much smaller than that of the Salton trough family (Fig. A1h). We also note that the San Gabriel family has roughly isotropic shape (reminiscent of explosion) whereas the Salton trough family is concentrated in a small number of directions (suggesting flow in specific channels). To conclude, our results suggest that the cluster structure is stable with respect to the magnitude threshold of the nearest-neighbor analysis.

Section B. ***Normalized tree depth***

The main text of the paper analyzes the average leaf depth $\langle d\rangle$. An alternative approach to treat the bimodal distribution of the average leaf depth is related to the depth scaling with family size N. Note that a linear chain of size N has depth $\langle d\rangle = N-1 \sim N$; a perfect spray-shaped tree of size N (a tree with $N-1$ leaves directly attached to the root) has depth $1 \sim N^0$. Here the sign "~" stands for "scales as when N increases". It is hence natural to expect for the observed trees to behave like $\langle d\rangle \sim N^{\kappa}$, with $0 < \kappa < 1$. Figure B1a shows the average leaf depth $\langle d\rangle$ as a function of the family size N for the regular families obtained in the nearest-neighbor analysis for $m \geq 2$ earthquakes. The figure only shows 452 families with the mainshock magnitude 4.0 or above. A notable observation is the existence of two principal modes of the expected increase of the depth $\langle d\rangle$ with family size N; they are depicted by two lines $\langle d\rangle \propto N^{0.5}$. One of the modes (located to the left) corresponds to the much higher tree depths for the same family size. To quantify the mode separation, we introduce the normalized tree depth $\delta = \langle d\rangle\times N^{-0.5}$, which balances the effect of depth increase with the family size. Figure B1b further illustrates the modes of the depth-size dependence, using different levels of the normalized depth δ. Figure B2 shows three examples of trees with different values of the normalized depth δ.

We note that the tree structure is affected by the magnitude of the events in the family. In particular, large-magnitude events tend to attract more offspring, according to the nearest-neighbor distance of Eq. (1) that exponentially decreases with the magnitude of the parent. Figure B3 shows the normalized depth δ as a function of the family mainshock magnitude m for the 51 regular families of size $N \geq 100$. The values of the normalized depth span the range $0.05 < \delta < 2$. Notably, there exists a *transition in the family formation* process between medium-magnitude and large-magnitude events with the transition range $4.7 < m < 6.2$. Namely, *all* $m > 6.2$ mainshocks form prominently spray-shaped clusters with very small tree depth, $\delta < 0.11$; such clusters would be commonly referred to as *aftershock sequences*. We note that large-magnitude events typically break the entire seismogenic zone and reach the free surface; this may be related to the topologic structure of the respective families. *All* medium-magnitude mainshocks, $m < 4.7$, form families with high normalized depth, $\delta > 0.5$; such clusters would be commonly referred to as *swarms*. Finally, the mainshocks in the transition range $4.7 < m < 6.2$ may form clusters with a wide variety of normalized depths, $0.05 < \delta < 2.0$, which includes linear (for $\delta > 0.5$) and spray-shaped (for $\delta < 0.2$) families as well as all intermediate types ($0.2 < \delta < 0.5$).

Section C. *Cluster statistics vs. average leaf depth*

We have noticed already in Sect. 3 that some family statistics considered in our analysis are related to each other. Say, it is natural to expect the topological depth $\langle d \rangle$ to be negatively associated with the family branching index B. We demonstrate in this section that numerous statistical properties of the nearest-neighbor families are indeed strongly coupled with the average leaf depth $\langle d \rangle$. Such coupling in many cases is a natural consequence of conditional family construction, and hence presents purely statistical rather than physical effect. Nevertheless, systematic exploration of these dependencies seems necessary for better understanding of the earthquake family structure. We choose the topological depth ‹*d*› as the governing parameter since it exhibits the strongest association with the regional properties among the examined family statistics not exclusively related to foreshocks (see Fig. 7, Table 1).

The frequency-magnitude distribution for cluster mainshocks in two groups with different ranges of family depth ‹*d*› is shown in Fig. C1. The mainshock distribution within the topologically shallow families (solid line) is reminiscent of that for the entire mainshock population [cf. ZBZ13, Fig. 10] and can be closely approximated by the exponential Gutenberg-Richter law with b-value (slope of the line) $b = 1$. The mainshocks of the topologically deep families (dashed line) also follow an exponential distribution, although with significantly lower b-value $b \approx 0.6$. Accordingly, the proportion of large-magnitude mainshocks is higher within topologically deep, swarm-like families. Recall that the b-value can be interpreted as $b = 0.5d_f$ with d_f being the fractal dimension of epicenters [*Aki*, 1981]. This implies that the epicenters of the burst-like families with small topological depth occupy statistically the entire surface ($d_f \approx 2$), while those of the swarm-like families occur within essentially one-dimensional channels ($d_f \approx 1.2$). This property is explicitly confirmed below in Fig. C10. Another interesting observation is that while the number of swarm-like low-magnitude clusters is much smaller than the number of burst-like low-magnitude clusters; the number of large-magnitude clusters is comparable for both cluster types.

Figure C2 shows the average number of aftershocks and foreshocks per family, in regular analysis for events with small-to-intermediate mainshock magnitudes $2 \le m \le 6$, as a function of family mainshock magnitude m. The analysis is done separately for deep families ($\langle d \rangle > 5$, diamonds, dashed line) and shallow families ($\langle d \rangle \le 5$, circles, solid line). The average number of foreshocks and aftershocks is larger in deep families. This is true for aftershocks in families with mainshock magnitude $m \le 5$, and for foreshocks in families with mainshocks magnitude $m \le 6$. At the same time, the large magnitude families seem to have fore/aftershock productivity that is independent of the tree depth. The figure does not show mainshock magnitudes above 6, which add to the variability of the plot without changing the above conclusions. The average fore/aftershock number for intermediate mainshock magnitudes can be approximated by an exponential law

$$N = K_N \times 10^{\beta m}. \quad \text{(C1)}$$

The value of the productivity index for aftershocks in deep ($\langle d \rangle > 5$) and shallow ($\langle d \rangle \le 5$) families is $\beta \approx 0.7$, $\beta \approx 0.9$ respectively; these estimates are done within the magnitude range [2.5-5] and may be different if larger mainshocks are considered. While it is harder to estimate the productivity index for foreshocks due to large fluctuations of the foreshock number, it is safe to say that the index value is close to $\beta = 0.5$ for the mainshock magnitude range [2.5-5].

In part I of this study it was shown [ZBZ13, Fig. 14] that the average number of aftershocks per family N_A, ignoring the family depth, scales with the mainshock magnitude m as $N_a \propto 10^{\beta m}$, $\beta \approx 1$; this result is consistent with the other studies that report the productivity index α of about unity [e.g., *Helmstetter et al.*, 2005]. The depth-independent index $\beta \approx 1$ may seem inconsistent with the depth-dependent indices $\beta \approx 0.7$ and $\beta \approx 0.9$, which are both significantly less that unity. This effect is explained by the depth-dependent mainshock distribution illustrated in Fig. C1. Namely, the proportion of topologically deep low-magnitude clusters is small; hence, the total number of aftershocks for low-magnitude clusters is about the same as the number of aftershocks for shallow low-magnitude clusters. At the same time, the proportion of topologically deep large-magnitude clusters is much larger; hence, the total number of aftershocks for large-magnitude clusters is the sum of that number in both deep and shallow clusters. This effect leads to increase of the scaling exponent in the entire population compared to the subpopulations of deep and shallow clusters.

In part I it was shown [ZBZ13, Fig. 15] that the aftershock and foreshock productivity in Δ-analysis is independent of the family mainshock magnitude. This motivates examination of the average number of Δ-foreshocks and Δ-aftershocks per family grouped by the family depth. The results are shown in Fig. C3a, where all families are divided into 5 equal percentile groups according to the increasing value of the average leaf depth $\langle d \rangle$. The number of foreshocks and aftershocks clearly increases with the topological depth. At the same time, the number of foreshocks is always less than the number of aftershocks. Figure C3b shows the proportion of Δ-foreshocks in the families with size $N \geq 10$, according to the average leaf depth $\langle d \rangle$. The proportion of foreshocks increases with the depth from almost 0 for shallow families to above 0.25 for the deepest ones.

Next, we focus on the temporal intensity of events within a family around the mainshock. Figure C4 shows the estimated earthquake intensity, in events per day per cluster, in regular clusters with mainshock magnitude $m \geq 4$ within 30 days from a mainshock. The analysis is done separately for shallow clusters ($\langle d \rangle \leq 5$, solid line, circles) and deep clusters ($\langle d \rangle > 5$, dashed line, diamonds). This analysis includes clusters with no foreshocks and/or aftershocks. The intensity of events decreases away from the mainshock, in agreement with the depth-independent results [ZBZ13, Fig. 16]. The intensity of topologically deep clusters is order of magnitude higher than that of shallow ones (consistent with the results of Fig. C3), independently of the time away from mainshock. Moreover, the intensity of events decays faster within 10 days from the mainshock (for both foreshocks and aftershocks) in shallow clusters. This visual impression is confirmed by the analysis of Fig. C5 below. We note also that the foreshock intensity for shallow clusters is always below 0.1 event/day/cluster, and it decreases to 0.01 events/day/cluster 10 days away from a mainshock. This explains the observation that only 27% of the shallow clusters ($\langle d \rangle \leq 5$, $m \geq 4$) have foreshocks; while among the deep clusters ($\langle d \rangle > 5$, $m \geq 4$) 95% have foreshocks.

Figure C5 presents more focused results on event intensity within 10 days from mainshocks for families with at least one Δ-aftershock or Δ-foreshock; the earthquake intensity is measured in events per day per family. The aftershock decay in the examined cases closely follows the Omori-Utsu law [*Omori*, 1894; *Utsu et al.*, 1995]:

$$\Lambda = K_\Lambda \times (t + c)^{-p}. \quad \text{(C2)}$$

The decay rate is higher for topologically shallow families ($p \approx 0.85$) than for deep ones ($p \approx 0.65$). The foreshock decay shows much more scattered results due to smaller number of events, but it can also be coarsely approximated by a power law. Due to sampling problems, we are not trying to estimate the exact foreshock decay rates, although it is clear that the overall decay in shallow families is faster than in deep ones. For visual convenience we show in Fig. C5b two lines that correspond to power law decay with rates of 0.65 and 1.1. The results are consistent with the depth-independent intensity decay illustrated in Fig. 17 of ZBZ13. The results confirm the suggestion in Fig. C4 that the intensities of events in topologically shallow sequences tend to decay faster as time from mainshock (in both directions) increases.

Figure C6 illustrates results of regular analysis of the magnitude difference Δ_m between the mainshock and the largest foreshock (diamonds, dashed line) and aftershock (circles, solid line). The magnitude difference for both event types tends to be smaller for deeper families; the effect although is much stronger for aftershocks than for foreshocks. Notably, the depth-dependent magnitude difference for the foreshocks is always statistically indistinguishable from the depth-independent average of $\Delta_m = 1.2$ [see ZBZ13, Fig. 18]. In contrast, the depth-dependent magnitude differences for aftershocks do deviate significantly from the depth-independent average $\Delta_m = 1.1$ for very shallow and very deep families.

The duration of foreshocks and aftershocks in Δ-analysis is illustrated in Fig. C7; both foreshock and aftershocks sequences are longer for deep families. The duration of

Δ-foreshocks is order of magnitude smaller than that of Δ-aftershocks, independently of the family depth. The distribution of the area for aftershock sequences according to the family depth is shown in Fig. C8. The area tends to increase with increasing topological depth, in agreement with the example results shown in Figs. 1 and 2 (see also Figs. A1, A2). The dependence of area on the family depth is more scattered than the other characteristics examined in this study; this prevents a robust analysis of the foreshock area.

Next, we examine the immediate child productivity by analyzing the average number B of children per parent (Fig. C9). In graph-theoretical terminology, this is known as the *branching number*; in seismological context it is usually called *the number of first-generation offspring*. Specifically, we (i) consider *every* parent event within each family, (ii) focus on the first-generation offspring only, and (iii) do not consider events with no children, so the minimal number is $B = 1$. The branching numbers are averaged within each family. Fig. C9a shows that the shallow families have a prominently higher average B. This observation is further illustrated in Fig. C9b that displays the distribution of B for shallow ($\langle d \rangle \leq 3$) and deep ($\langle d \rangle > 3$) families. As shown, the distribution of B for deep families has exponential tail $1-F(B) = C_B \times 10^{-\alpha B}$ with $\alpha \approx 0.3$.

Finally, we analyze the directional dependency of events in families of different types. Specifically, consider the empirical distribution $F(\theta)$ of the surface angle θ between the epicenters of family mainshock and the other events. The angle, in degrees, is counted counterclockwise assuming that East corresponds to $\theta = 0$. For each family we perform a one sample Kolmogorov-Smirnov test [*Conover*, 1971] that compares $F(\theta)$ to the uniform distribution on the interval [0, 360]. The proportion U of families with at least 5 events and mainshock $m \geq 4$ that pass this test at level 0.01 (we call such families *isotropic*) for different average leaf depths is shown in Fig. C10. The proportion of isotropic families decreases as the tree depth increases. In other words, burst-like sequences develop in spatially isotropic fashion reflected in uniform circular event distribution, while deeper swarm-like sequences propagate along preferred channels in particular directions. The existence of preferred propagation channels may also explain the observation of Fig. C8 that the area of aftershock sequences increases with the family depth (and related results in Figs. 1 and 2); a failure cascade along specific (presumably weaker) directions can extend larger distance from the mainshock compared to the isotropic failures characterizing the burst-like shallow sequences.

Section D. ***ETAS model: specification and parameters***

The ETAS model is specified in terms of the conditional intensity $\lambda(t,\mathbf{f},m|H_t)$ of a process $Z_t=\{t_i,\mathbf{f}_i,m_i\}$ given its history $H_t = (\{t_i,\mathbf{f}_i,m_i\} : t_i < t)$ up to time t. Here t_i represents earthquake occurrence times, $\mathbf{f}_i$ their coordinates (e.g., epicenter, hypocenter, or centroid) and m_i the magnitudes [*Daley and Vere-Jones*, 2002]. The statistical analysis and inference for Z_t are done using the conditional likelihood

$$\log L_t = \sum_{t_i<t} \log \lambda\left(t_i, \mathbf{f}_i, m_i \,|\, H_t\right) - \int_0^t \int_M \int_F \lambda\left(t, \mathbf{f}, m \,|\, H_t\right) dt\, dm\, d\mathbf{f}, \qquad \text{(D1)}$$

where M and F denote the magnitude range and spatial domain of events, respectively. We assume furthermore that the magnitudes of events are independent and drawn from the Gutenberg-Richter (exponential) distribution with a constant b-value. This reduces conditional intensity to the following special form, which allows various particular parameterizations [*Ogata*, 1998, 1999]:

$$\lambda(t,\mathbf{f}|\mathrm{H}_t) = \mu_0(t,\mathbf{f}) + \sum_{i:t_i<t} g(t - t_i, \mathbf{f} - \mathbf{f}_i, m_i).$$

We use in this study a homogeneous background intensity $\mu_0 = \mu$ and the following parameterization for the response function g suggested by *Ogata* [1998, Eq. (2.3)]:

$$g(t,x,y,m) = \frac{K}{(t+c)^p}\frac{\exp(\alpha(m - m_0))}{(x^2+y^2+d)^q}. \qquad \text{(D2)}$$

Here m_0 is the lowest considered magnitude, and (x,y) are Cartesian coordinates of the epicenters. The model is specified by 8 scalar parameters θ □□□μ, □□ K, c, p, α, d, q□. In this study, we generate synthetic ETAS catalogs using parameters consistent with those reported in the literature [e.g., *Wang et al*., 2010; *Chu et al*., 2011; *Marzocchi and Zhuang*, 2011]: μ = 0.003 (km^2 year)$^{-1}$, b = α = 1, K = 0.007 (km^2 year)$^{-1}$, c = 0.00001 year, p = 1.17, q = 1.7, d = 30 km^2; the simulations are done within a region of 500×500 km during 15 years. The catalog consists of 146,432 earthquakes.

Section E. *Analysis of Variance: Review*

The *one-way* ANOVA test (*Freedman*, 2005) compares the means of several groups of observations by examining the variance within the groups relative to the variance between the groups. Formally, consider samples X_{ij}, where index i = 1,…,G counts different groups and index j = 1,…,N_i counts observations within group i; and let $N = N_1 + \ldots + N_G$. Let $\bar{X}_i$ denote the sample average for the group i and μ_i denote the population mean for the same group. The ANOVA tests the null hypothesis H_0: $\mu_1 = \ldots =$

μ_G vs. the alternate hypothesis that at least two groups have different means. The test statistic is computed as

$$F = \frac{SSG}{SSE}\frac{N-1}{G-1},$$

where *SSG* is the *group sum of squares* and *SSE* is the *error sum of squares*:

$$SSG = \sum_{i=1}^{G} N_i \left(\bar{X}_i - \bar{X}\right)^2 ;\ SSE = \sum_{i=1}^{G}\sum_{j=1}^{N_i}\left(X_{ij} - \bar{X}_i\right)^2 .$$

The intuition behind the test is that if all groups have the same mean, then SSG/(G-1) ≈ SSE/(N-1) and the test statistic *F* should be close to unity; while if the groups have different means, then SSG/(G-1) < SSE/(N-1) and the values of *F* will increase. Namely, if (i) the observations are normally distributed and (ii) the variances of all the groups are the same, then the test statistic *F* has *F*-distribution with (*G*-1) and (*N*-1) degrees of freedom (*Freedman*, 2005). The ANOVA test is reasonably robust with respect to the violation of both the above assumptions and it is known to have large power with respect to numerous alternative hypotheses. When applying the ANOVA test, we always transform the variables to make the samples approximately Normally distributed.

Table C1: Earthquake cluster statistics related to the earthquake family type

Statistic	Burst-like family	Swarm-like family	Figure #	
			Δ-analysis*	Regular analysis
Average leaf depth, $\langle d \rangle$	Low	High	1-4	
b-value for mainshocks	High	Low	C1	
Ave. no. of aftershocks per family, N_a	Low	High	C3	C2a
Ave. no. of foreshocks per family, N_f	Low	High	C3	C2b
Intensity of aftershocks, Λ_a	Low	High	C4, C5a	
Intensity of foreshocks, Λ_f	Low	High	C4, C5b	
Magnitude difference between mainshock and largest aftershock, Δ_m	High	Low		C6
Magnitude difference between mainshock and largest foreshock, Δ_m	High	Low		C6
Duration of aftershocks, D_a	Low	High	C7a	
Duration of foreshocks, D_f	Low	High	C7b	
Area of aftershocks, A_a	Low	High	C8	
Branching index, B	High	Low		C9
Angular surface isotropy, U	High	Low		C10

* Defined in Sect. 2 of ZBZ13

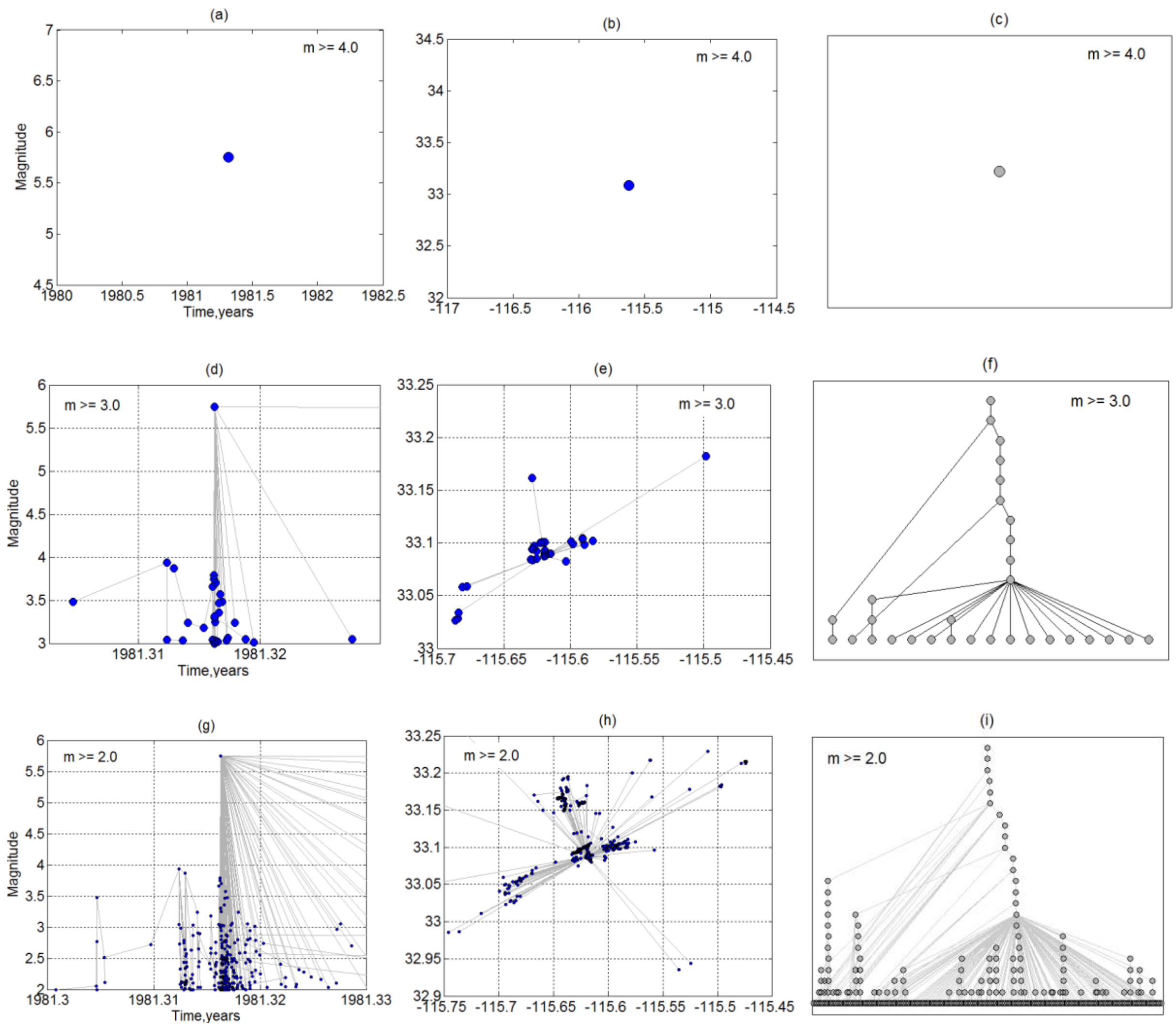

Figure A1: Cluster in Salton trough area. Circles correspond to earthquakes, lines to parent links. Figure shows results for different magnitude thresholds of the nearest-neighbor analysis: (a,b,c) $m \geq 4.0$, (d,e,f) $m \geq 3.0$, (g,h,i) $m \geq 2.0$. (a,d,g) Magnitude as a function of time. (b,e,h) Space map. (c,f,i) Topologic tree.

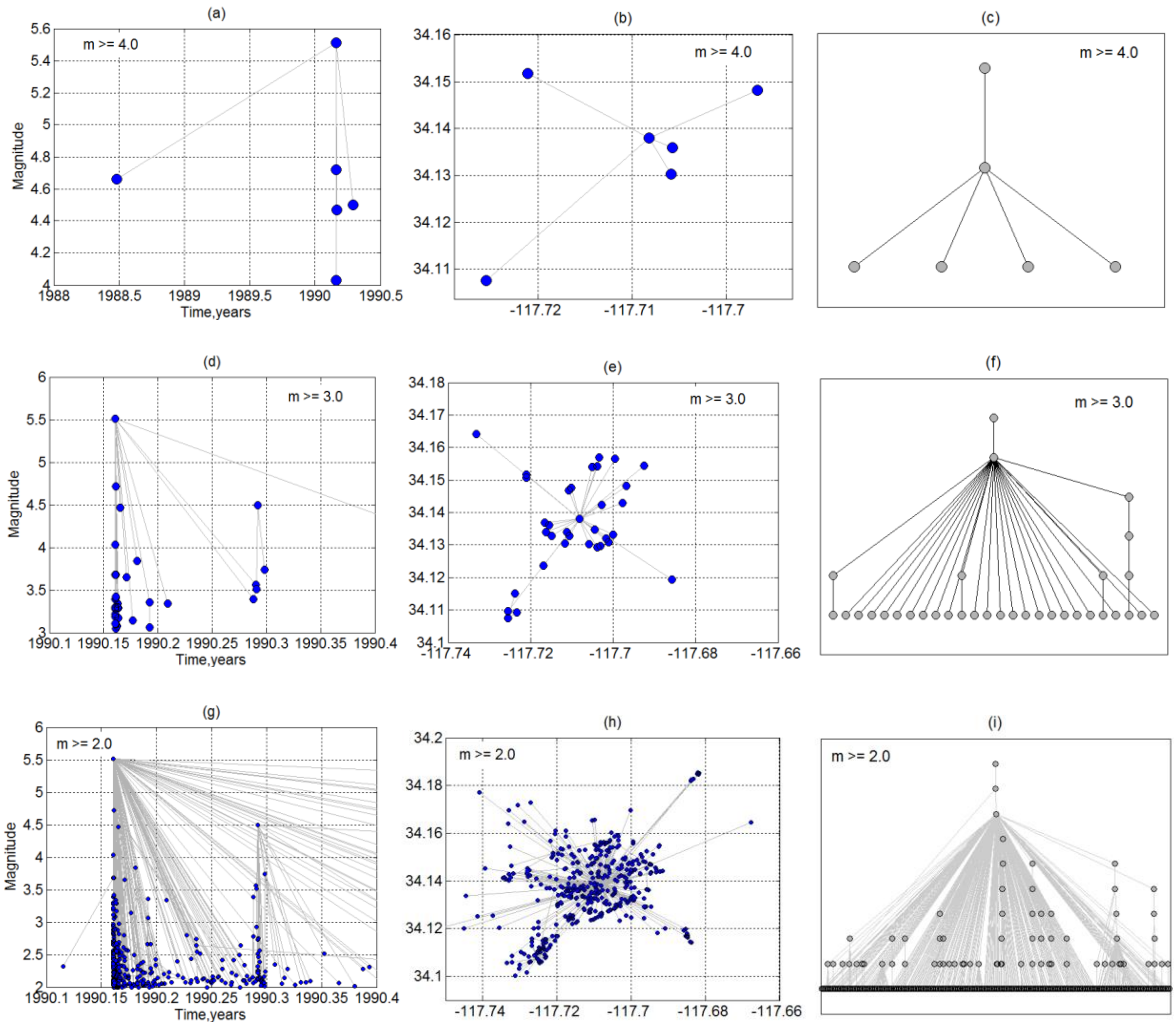

Figure A2: Family in San Gabriel area. The other notations are the same as in Fig. A1.

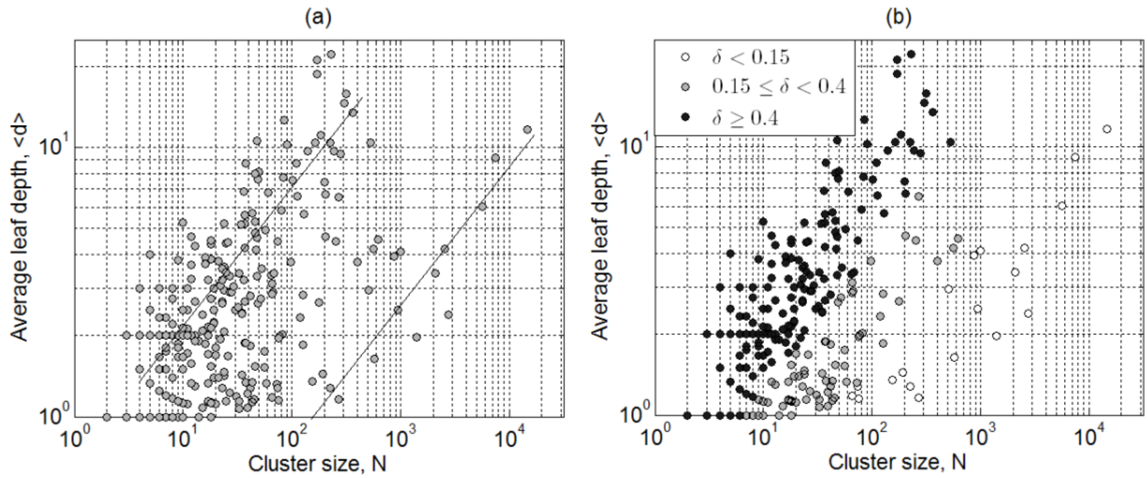

Figure B1: Two types of nearest-neighbor families. The figure shows the average leaf depth ‹*d*› as a function of the family size *N* for 452 regular families with maximal magnitude $m \geq 4$. The nearest-neighbor analysis is done for $m \geq 2.0$. Panel (a) depicts the two modes by lines $\langle d \rangle \propto N^{0.5}$: one of the modes is characterized by much larger average leaf depth for the same family size. Panel (b) further illustrates the two modes by using different colors for families with different normalized depth $\delta = \langle d \rangle \times N^{-0.5}$, as described in the legend.

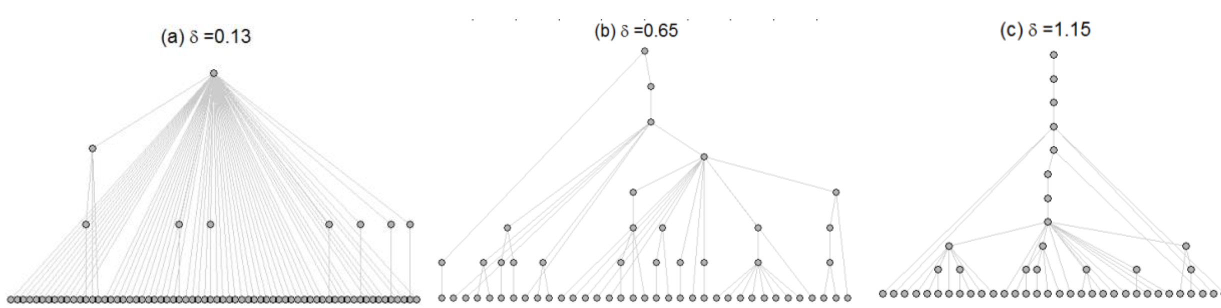

Figure B2: Examples of trees with different values of the normalized tree depth δ. All trees correspond to the earthquake families observed in southern California.

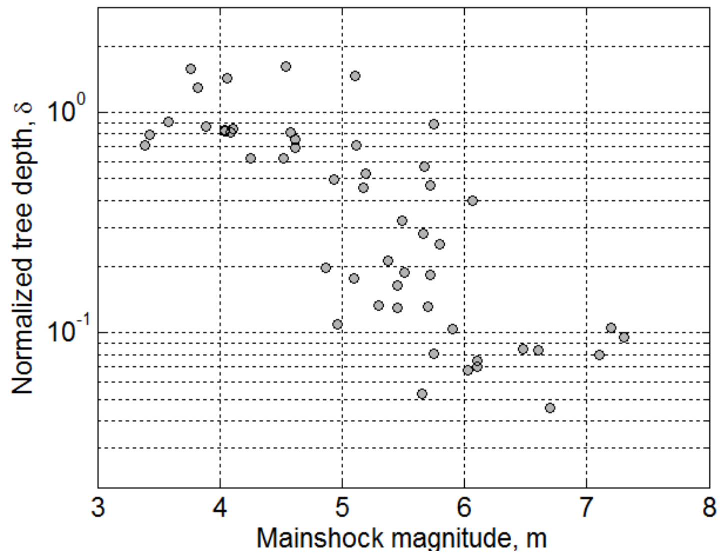

Figure B3: Two types of nearest-neighbor families. The figure shows the normalized tree depth δ as a function of the family mainshock magnitude *m* for 51 regular families with size $N \geq 100$. There exists a transition in the family formation process: all mainshocks with $m < 4.7$ correspond to large-depth trees (swarm-like families), $\delta > 0.5$; all mainshocks with $m > 6.2$ correspond to small-depth trees (burst-like families), $\delta < 0.11$; the mainshocks in the transition range $4.7 < m < 6.2$ may form families of various types, with $0.05 < \delta < 2$.

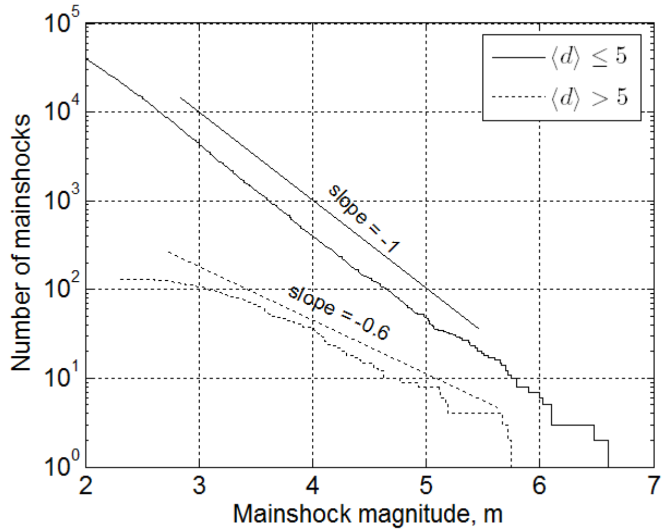

Figure C1: Number of mainshocks with magnitude equal or above *m*. The analysis is done separately for clusters with average leaf depth $\langle d \rangle \leq 5$ (solid line) and $\langle d \rangle > 5$ (dashed line). Deep, swarm-like families have significantly larger proportion of high-magnitude mainshocks.

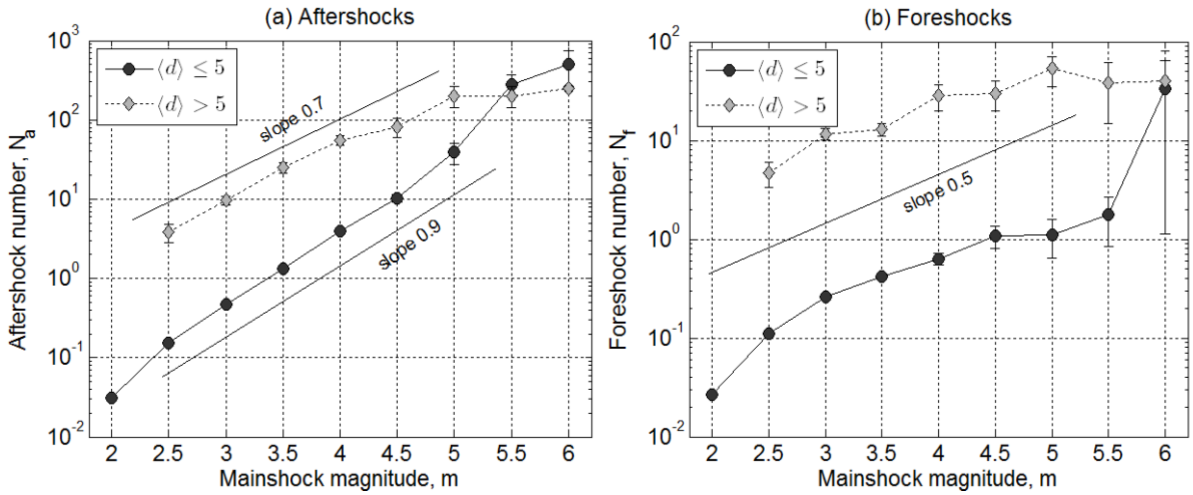

Figure C2: Average number of aftershocks (panel a) and foreshocks (panel b) per family for different mainshock magnitude. The analysis is done separately for shallow families, $\langle d \rangle \leq 5$, (solid line, circles) and deep families, $\langle d \rangle > 5$, (dashed line, diamonds). The productivity is significantly larger in deep families.

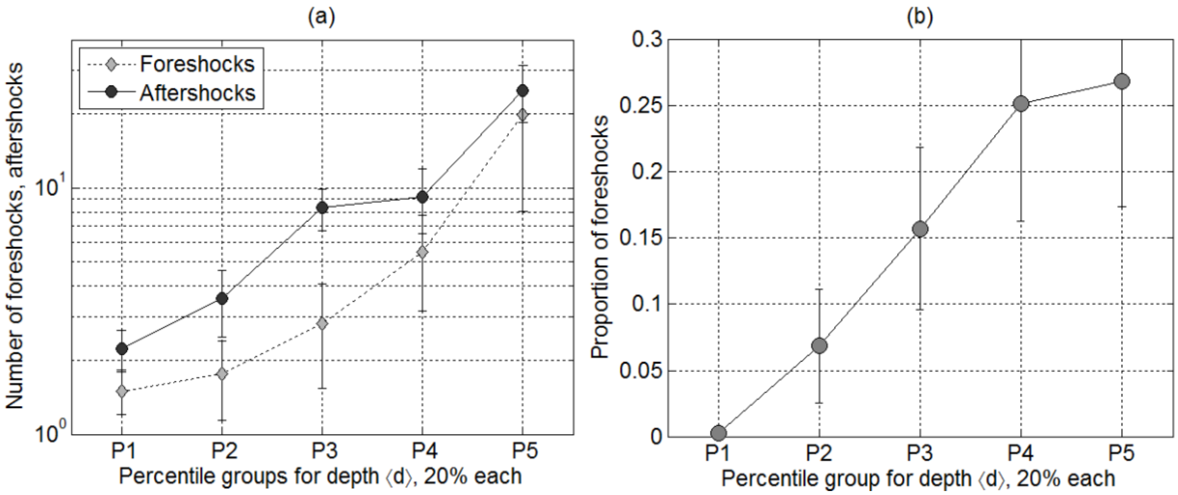

Figure C3: (a) Average number of Δ-foreshocks (diamonds, dashed line) and Δ-aftershocks (circles, solid line) for families with different average leaf depth $\langle d \rangle$. Each group corresponds to 20% of the families in Δ-analysis, according to the increasing $\langle d \rangle$-values. Only families with at least one fore/aftershock are examined. Each foreshock group contains 25 or 26 families; each aftershock group contains 27 or 28 families. The error bars correspond to a 95% confidence interval for the mean. (b) Proportion of foreshocks in Δ-families with size $N \geq 10$. Each group contains 22 or 23 families.

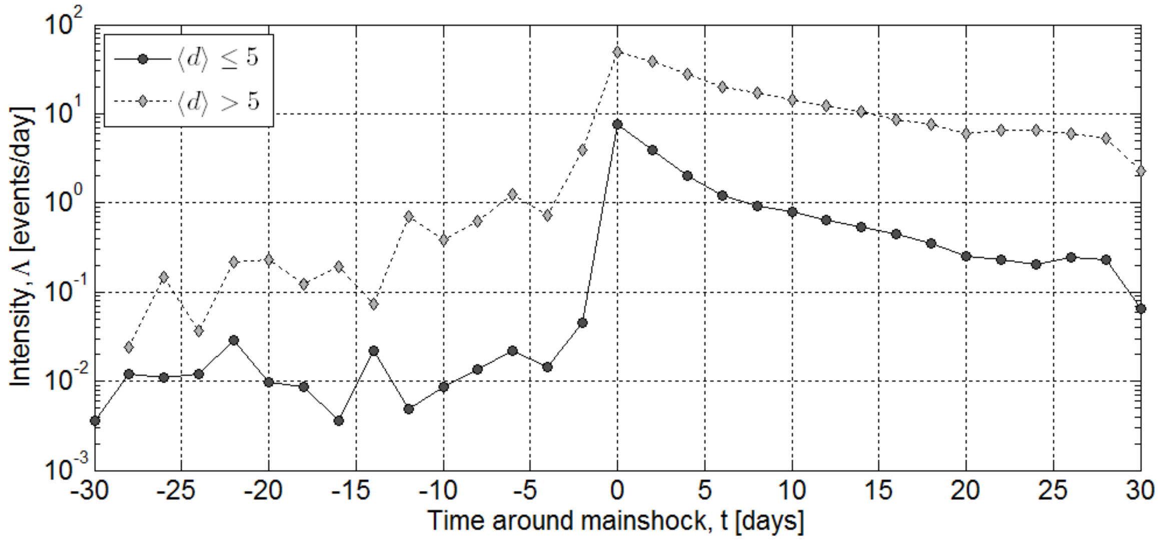

Figure C4: Intensity Λ of events around a mainshock in events per day per cluster; regular analysis, clusters with mainshocks $m \geq 4$. The analysis is done separately for clusters with ‹d› ≤ 5 (solid line, circles) and ‹d› > 5 (dashed line, diamonds).

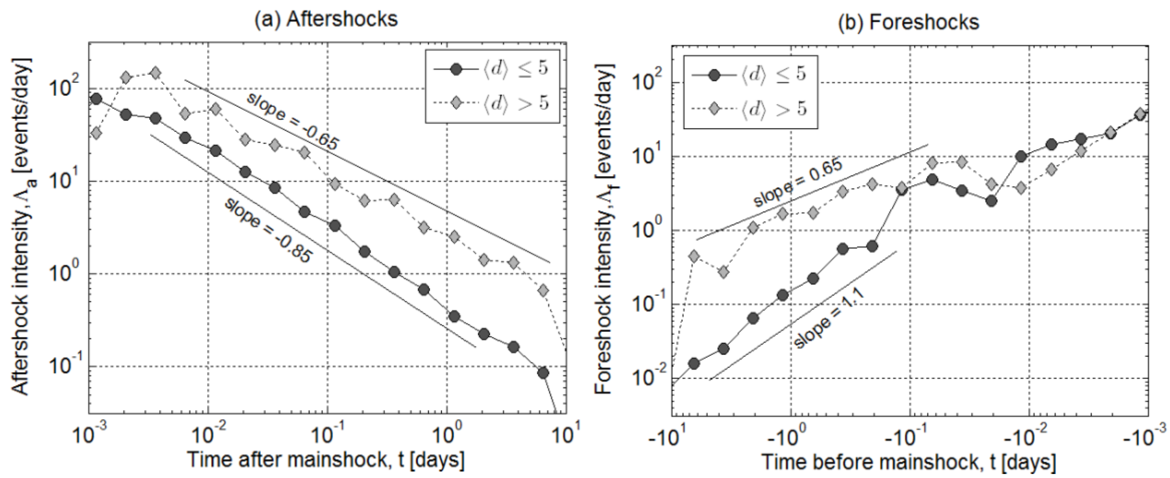

Figure C5: Intensity of aftershocks (panel a) and foreshocks (panel b) in events per day per family for families with mainshock magnitude $m \geq 4$ and at least one aftershock (panel a) or foreshock (panel b) in Δ-analysis. The analysis is done separately for families with $\langle d \rangle \leq 5$ (solid line, circles) and $\langle d \rangle > 5$ (dashed line, diamonds). The event decay away from the mainshock is more rapid in topologically shallow families.

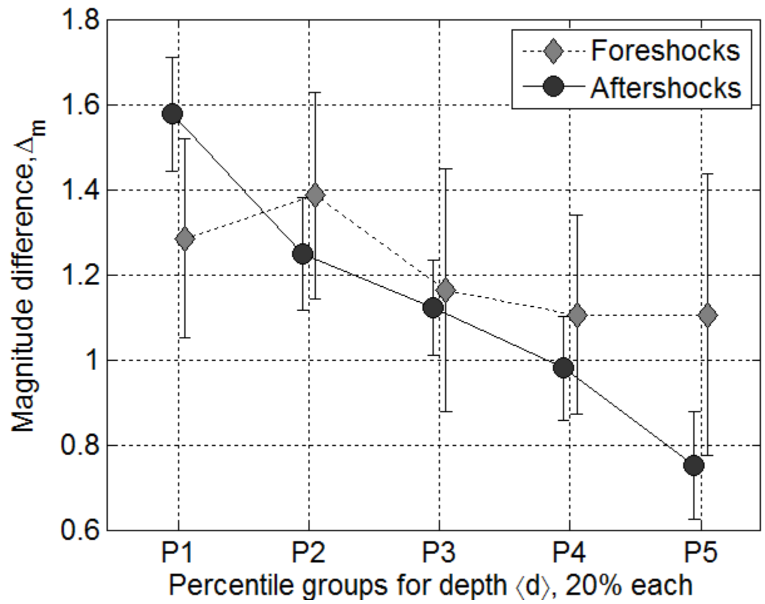

Figure C6: Magnitude difference Δ_m between the mainshock and the largest foreshock (dashed line, diamonds) and aftershock (solid line, circles) in regular analysis. The figure shows the average value of the magnitude difference for different ranges of the average leaf depth $\langle d \rangle$ in regular analysis. Each depth group corresponds to 20% of families with at least one fore/aftershock. Each aftershock group contains 67 or 68 events; each foreshock group contains 25 or 26 events. The error bars correspond to a 95% confidence interval for the mean.

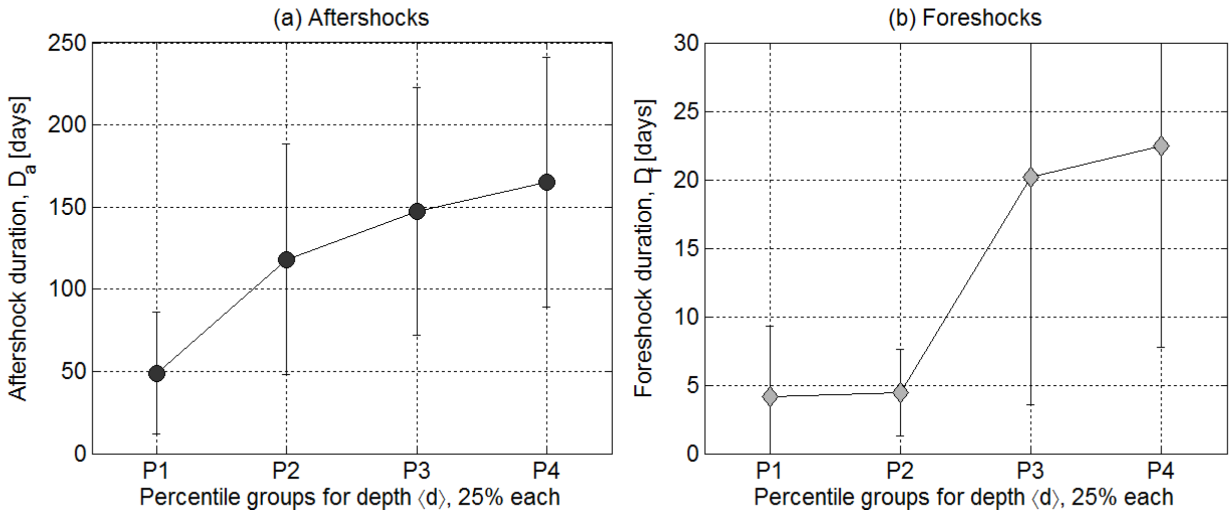

Figure C7: Duration of foreshock and aftershock sequences. The figure shows the average value of duration for different ranges of the average leaf depth ‹*d*› in Δ-analysis. Each depth group corresponds to 25% of families with at least one fore/aftershock. (a) Aftershocks, each group contains 84 or 85 sequences. (b) Foreshocks, each group contains 32 sequences. The error bars correspond to a 95% confidence interval for the mean.

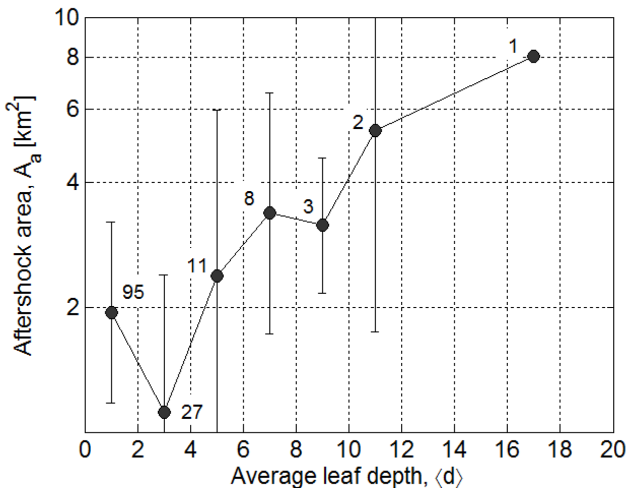

Figure C8: Area *A* occupied by aftershocks. The analysis only considers Δ-families with at least 5 aftershocks within 5 parent fault rupture lengths from the mainshock. The area is averaged over all families within different ranges of the average leaf depth, each range has length 2. The number of families within each range is indicated in figure.

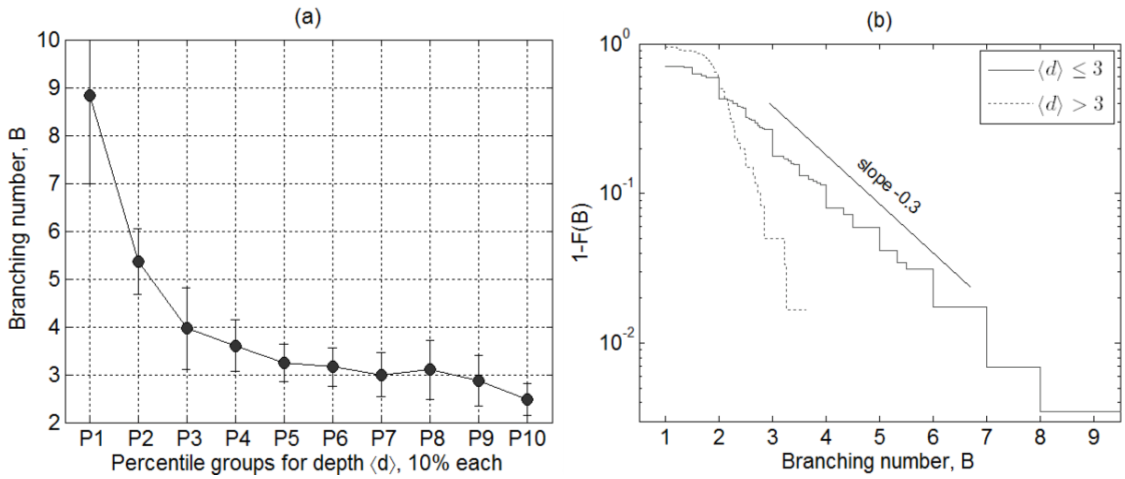

Figure C9: Branching number *B*. (a) The average value of the branching number for different ranges of the average leaf depth ‹*d*› in regular analysis. Each depth group corresponds to 10% of families with mainshock magnitude $m \geq 4$ and size $N \geq 10$. Each group contains 19 or 20 families. The error bars correspond to a 95% confidence interval for the mean. (b) The tail of the distribution of the branching number *B* for families with ‹*d*› ≤ 3 (solid line) and ‹*d*› > 3 (dashed line). Branching is larger for shallow families.

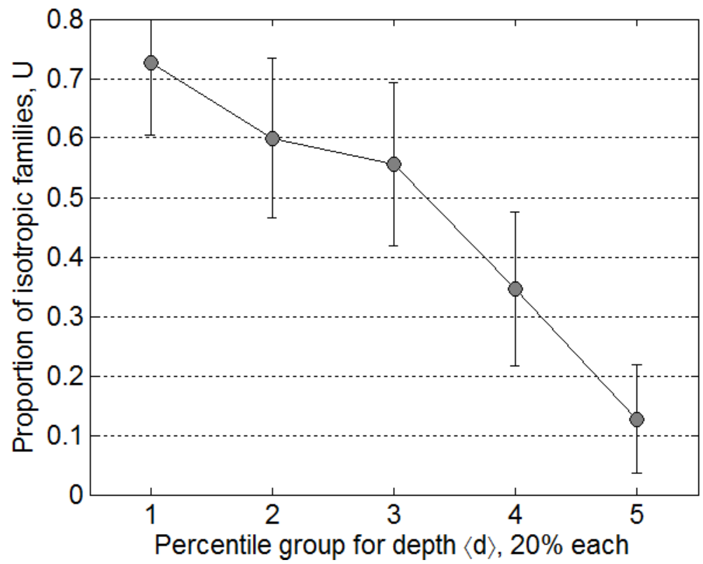

Figure C10: Circular spatial isotropy of family events. The figure shows the proportion of families with circularly uniform distribution of events relative to the mainshock, according to the Kolmogorov-Smirnov test at level 0.01 (see the text for details). Regular families with at least 5 events and mainshock magnitude $m \geq 4$ are considered. The results are averaged within families with different values of the average leaf depth, each point corresponds to 20% of examines families; each group contains 54 or 55 families.